Bayesian Model Updating and Class Selection of a Wing-Engine Structure with Nonlinear Connections using Nonlinear Normal Modes

Mingming Song[1], Ludovic Renson[2], Babak Moaveni[1], and Gaetan Kerschen[3]

[1]*Dept. of Civil and Environmental Engineering, Tufts University, Medford, MA, USA*
[2]*Dept. of Mechanical Engineering, Imperial College London, London, UK*
[3]*Dept. of Aerospace and Mechanical Engineering, University of Liege, Liege, Belgium*

Abstract

This paper presents a Bayesian model updating and model class selection approach based on nonlinear normal modes (NNMs). The performance of the proposed approach is demonstrated on a conceptually simple wing-engine structure. Control-based continuation is exploited to measure experimentally the NNMs of the structure by tracking the phase quadrature condition between the structural response and single input excitation. A two-phase Bayesian model updating framework is implemented to estimate the joint posterior distribution of unknown model parameters: (1) at phase I, the effective Young's modulus of a detailed linear finite element model and its estimation uncertainty are inferred from the data; (2) at phase II, a reduced-order model is obtained from the updated linear model using Craig-Bampton method, and coefficient parameters of structural nonlinearities are updated using the measured NNMs. Five different model classes representing different nonlinear functions are investigated, and their Bayesian evidence are compared to reveal the most plausible model. The obtained model is used to predict NNMs by propagating uncertainties of parameters and error function. Good agreement is observed between model-predicted and experimentally identified NNMs, which verifies the effectiveness of proposed approach for nonlinear model updating and model class selection.

Keywords: Nonlinear model updating; nonlinear system identification; nonlinear normal modes; Bayesian inference; model class selection; uncertainty quantification and propagation; control-based continuation.

1. Introduction

Finite element (FE) models are arguably commonly used for structural design, assessment, and response prediction. The accuracy of FE models can be improved by inferring model parameters from *in-situ* measurements through a model updating process where model parameters are tuned to minimize the difference between measurements and the corresponding model predictions [1]. The discrepancies between model predictions and measurement data are mainly caused by three sources of uncertainty: (a) measurement noise, (b) modeling errors, and (c) model parameter uncertainty. Model updating directly reduces the model parameter uncertainty by integrating the model with measurement data. There have been numerous applications of model updating that employ a deterministic optimization approach [2-9]. In these applications, a least square problem is solved by minimizing an 'objective' or 'loss' function which consists of the difference between model predictions and measurements. One of the main shortcomings for the optimization approach

is that the method does not provide a measure of estimation uncertainty for the updating parameters. Probabilistic model updating approaches such as those using Bayesian inference have been developed to overcome this shortcoming. Bayesian model updating updates the prior distribution of model parameters to the posterior distribution using the likelihood of observed measurements. The posterior distribution provides the parameter uncertainty and the most likely values of parameters as the *maximum-a-posteriori* (MAP) estimate. This approach can also be applied to locally identifiable or even unidentifiable problems [10] by stochastic sampling of the posterior distribution. Several applications of Bayesian model updating exist in the structural dynamic literature [11-15]. Ntotsios et al. applied Bayesian damage identification on a numerical study of a highway bridge and a laboratory small-scaled bridge section [16]. Lam et al. implemented a Bayesian model updating of a coupled-slab system using field test data and an enhanced Markov chain Monte Carlo simulation algorithm [17]. Behmanesh and Moaveni performed probabilistic identification of simulated damage (added concrete block on the deck) on the Dowling Hall footbridge through a Bayesian finite element model updating [18]. Recently, a hierarchical Bayesian model updating has been proposed to provide realistic parameter uncertainty by estimating the distribution parameters as hyper-parameters [19-22]. The hierarchical framework is especially suitable when structural properties vary due to changing ambient or environmental conditions.

Many of the above applications have considered linear dynamic systems. While some studies included material nonlinearity [23-27], linear modal properties were still used as data features in model updating. In this paper, features called 'nonlinear normal modes' (NNMs) are used to update a nonlinear model and estimate the uncertainty of model parameters. NNMs extend the concept of linear normal modes to nonlinear systems [28-30]. NNMs have received increased attention in recent years as they provide a rigorous theoretical framework for interpreting many nonlinear dynamic phenomena [31-33]. For instance, NNMs can be used to predict the amplitude of the response of a nonlinear structure at resonance, i.e., when the risk of structural failure is the greatest. The identification of NNMs using broadband excitation was proposed in [34], but phase resonance testing remains so far the most popular approach [35]. Phase resonance testing aims to isolate one NNM at a time by reaching a phase quadrature condition between the response and the applied excitation. For nonlinear structures, this quadrature condition is difficult to reach due to the presence of bifurcations and the propensity of the structure to jump between coexisting stable responses. Several methods such as control-based continuation (CBC) and phase-locked loops were proposed to address these issues [36, 37]. In this study, CBC is used to find responses that satisfy the phase quadrature condition and track their evolution as the excitation amplitude is increased. The so-called backbone curves obtained in this way correspond to the NNMs of the underlying conservative system provided that the excitation is appropriately distributed in space and frequency [35, 38].

NNMs identified experimentally can be compared to NNMs calculated from the nonlinear model of the structure. In this paper, the harmonic balance method (HBM) [39] is used to compute NNMs, although several other methods exist and could have been used [40]. Particular advantage of the HBM is that the number of harmonics used to approximate the response of the structure can

be reduced to filter out modal interactions and reduce computational load, thereby simplifying the calculation of the error function between experimental and theoretical results.

Several contributions have considered NNMs for parameter estimation and nonlinear model updating. Peter et al. [41] employed optimization to minimize the difference between backbone curves measured using the phase resonance method and their analytical counterparts computed using the HBM. The nonlinear stiffness parameters of a single degree-of-freedom (DOF) oscillator were estimated using a similar method in [36]. Hill et al. [42] performed Bayesian model updating of nonlinear structures based on analytical models to describe the backbone curves. They derived analytical expression to describe the backbones which only provided an approximate solution and was limited to weakly nonlinear systems. Song et al. [43] implemented a numerical case study of Bayesian model updating on a nonlinear beam known as the COST Action F3 benchmark [44]. In that study, the NNMs were identified from simulated response under broadband excitation. The present paper demonstrates the model updating methodology proposed in [43] on a structure with multiple localized nonlinearities and using NNMs identified from experimental data. In addition, the present paper further exploits Bayesian inference to perform model class selection and choose the most plausible model (i.e., the model with the largest evidence) among a set of candidates. This approach has the benefit to combine nonlinearity characterization and parameter estimation - two steps which are usually considered as separate in the identification of nonlinear structures [45].

The Bayesian model updating and model class selection methodology proposed here proceeds in two phases to update the linear and nonlinear parts of the structural model separately. The proposed method is applied to a conceptually simple wing-engine structure with nonlinear connections. Two NNMs of the structure are identified using CBC through phase resonance testing. At phase I, a linear FE model is updated using the NNMs identified at the lowest energy level. A reduced-order model (ROM) is created based on the updated linear model and then used for nonlinear model updating in Phase II. At phase II, the ROM is combined with five different classes of nonlinearity function, and Bayesian model updating and class selection are performed to estimate the posterior distribution and evidence for each model class.

2. Bayesian Inference for Model Updating and Model Class Selection Based on NNMs

2.1 Bayesian Model Updating

This section presents the general framework of Bayesian model updating using NNMs. For simple structural models with small numbers of DOFs, linear and nonlinear parameters can be updated together to obtain the joint posterior distribution. However, for complex structural systems with many DOFs, the updating process may become computationally prohibitive as it entails a large number of NNMs computations from the numerical model, which can be a computationally demanding task. To avoid this issue, this paper implements a two-phase model updating approach in which the underlying linear system parameters are estimated first, and then a ROM of the updated linear system is generated and used for nonlinear model updating. Since the ROM has fewer DOFs than the original model, Bayesian updating of the nonlinear system through stochastic sampling is computationally feasible. This two-phase Bayesian updating process has been demonstrated through a numerical application to a nonlinear beam in a previous study [43].

2.1.1 Phase I: Updating of the underlying linear model

Linear modal properties such as natural frequencies and mode shapes have been extensively used for model updating of linear structures with reasonable successes [2-9]. When vibration amplitude is sufficiently small, the contribution of nonlinearity is assumed to be negligible. As such, the NNMs identified at the lowest vibration level 'resemble' the linear modes [29] and can be used to update the parameters of the underlying linear system. Note that if this assumption is not verified (due, for instance, to friction nonlinearities), additional testing is required to identify the underlying linear modes of the system, or this Phase I should be modified to account for the presence of such nonlinearities and the estimation of their parameters.

The classical Bayes' theorem can be written as:

$$p(\boldsymbol{\theta} \mid \mathbf{d}, M) = \frac{p(\mathbf{d} \mid \boldsymbol{\theta}, M)\, p(\boldsymbol{\theta} \mid M)}{p(\mathbf{d} \mid M)} \tag{1}$$

where $\boldsymbol{\theta}$ is the vector of updating model parameters, $\mathbf{d}$ refers to the measured data (e.g., NNMs), and M denotes a specific model class or model form. Left term in Eq. (1) is the joint posterior probability density function (PDF). $p(\mathbf{d} \mid \boldsymbol{\theta}, M)$ is referred to as the 'likelihood function' which represents the probability of observing measurements $\mathbf{d}$ given parameters $\boldsymbol{\theta}$, and $p(\boldsymbol{\theta} \mid M)$ is the prior PDF which reflects the prior knowledge or engineering judgement about updating parameters before measurements are taken. $p(\mathbf{d} \mid M)$ is called 'evidence' or 'marginal likelihood' which quantifies the plausibility of model class M in the view of measurements. Higher evidence value indicates higher plausibility given the measurements. The evidence term usually lacks analytical solution and is often computed numerically through stochastic sampling or estimated using the approximate approach presented in section 2.2. Currently it is treated as an unknown constant whose exact value is not required for evaluating the posterior PDF when Markov chain Monte Carlo (MCMC) sampling methods are used. When uninformative prior distribution is assumed, e.g., uniform distribution, then the prior PDF is also a constant term. The uniform prior function is selected in this study considering the large modeling errors, missing material specifications and the unknown properties of nonlinear connections. The uniform distribution bounds the parameter values within a reasonable range and prevents it going beyond feasible physics. Combing all constant terms as $\hat{c}$, the following formulation is derived:

$$p(\boldsymbol{\theta} \mid \mathbf{d}, M) = \hat{c}\, p(\mathbf{d} \mid \boldsymbol{\theta}, M) \tag{2}$$

The model class M is neglected in the following discussion to save the notation and will be introduced back in section 2.2 for model class selection.

For evaluation of the likelihood function, an error function is defined to represent the discrepancy between model-predicted and experimentally identified data features. In the first phase of model updating where $\boldsymbol{\theta}$ represents linear model parameters, the error function is defined based on natural frequencies and mode shapes as

$$e_{\lambda}^{m}(\boldsymbol{\theta}) = \tilde{\lambda}_m - \lambda_m(\boldsymbol{\theta}), \tag{3}$$

$$\mathbf{e}_{\phi}^{m}(\boldsymbol{\theta}) = \frac{\tilde{\boldsymbol{\Phi}}_m}{\left\|\tilde{\boldsymbol{\Phi}}_m\right\|} - a_m \frac{\Gamma\boldsymbol{\Phi}_m(\boldsymbol{\theta})}{\left\|\Gamma\boldsymbol{\Phi}_m(\boldsymbol{\theta})\right\|}, \tag{4}$$

where $e_{\lambda}^{m}(\boldsymbol{\theta})$ and $\mathbf{e}_{\phi}^{m}(\boldsymbol{\theta})$ are the error function terms for the natural frequency and the mode shape of mode *m*. $\tilde{\lambda}_m$ and $\tilde{\boldsymbol{\Phi}}_m$ are experimentally identified eigenfrequency ($(2\pi f)^2$ in which f is natural frequency in Hz) and mode shape. $\lambda_m(\boldsymbol{\theta})$ and $\boldsymbol{\Phi}_m(\boldsymbol{\theta})$ are their respective model-predicted counterparts. Γ is a selection matrix which picks corresponding components of $\boldsymbol{\Phi}_m(\boldsymbol{\theta})$ (which usually has more components than $\tilde{\boldsymbol{\Phi}}_m$ whose dimension depends on the number of deployed sensors) according to $\tilde{\boldsymbol{\Phi}}_m$, and consists of only 0 and 1 terms. a_m is a scaling factor to ensure the mode shapes are comparable [21, 43] and is equal to $\tilde{\boldsymbol{\Phi}}_m \cdot \Gamma\boldsymbol{\Phi}_m(\boldsymbol{\theta}) \Big/ \left(\left\|\tilde{\boldsymbol{\Phi}}_m\right\| \left\|\Gamma\boldsymbol{\Phi}_m(\boldsymbol{\theta})\right\|\right)$.

Based on the principle of maximum entropy, the error function is assumed to follow a zero-mean Gaussian distribution with standard deviations for the natural frequency and the mode shape error terms give by [18]

$$\sigma_{\lambda_m} = w_m \mathrm{CoV}_{\lambda} \tilde{\lambda}_m, \tag{5}$$

$$\sigma_{\phi_m} = \sqrt{N_s} w_m \mathrm{CoV}_{\lambda}, \tag{6}$$

where w_m are weights for different modes which can be determined based on measurement accuracy. In the experimental application of this paper, w_m is set to be one to provide equal weights for all the considered modes. CoV_{λ} refers to the coefficient-of-variation (ratio of standard deviation to mean value) of the experimentally identified eigenfrequency for mode *m*. N_s is the number of sensors deployed in the instrumentation and balances the weights between natural frequency and mode shapes, as it has been done in past studies [18, 43].

The error function components are often assumed to be statistically independent Gaussian distribution. This is a conservative assumption and will maximize the uncertainty of posterior PDF based on the principle of maximum entropy. Assuming the error functions are independent, the likelihood function is written as

$$p(\mathbf{d} \mid \boldsymbol{\theta}) = \prod_{i=1}^{n} p(\tilde{d}_i \mid \boldsymbol{\theta}) = \prod_{i=1}^{n} \frac{1}{\sqrt{2\pi}\sigma_i} \exp\left(-\frac{1}{2}\frac{e_i^2}{\sigma_i^2}\right) \propto \exp\left(-\frac{1}{2} J(\boldsymbol{\theta}, \mathbf{d})\right), \tag{7}$$

$$J(\boldsymbol{\theta}, \mathbf{d}) = \sum_{m=1}^{N_m} \left(\frac{e_{\lambda}^{m}(\boldsymbol{\theta})}{\sigma_{\lambda_m}}\right)^2 + \sum_{m=1}^{N_m} \frac{\mathbf{e}_{\phi}^{m}(\boldsymbol{\theta})^T \mathbf{e}_{\phi}^{m}(\boldsymbol{\theta})}{\sigma_{\phi_m}^2}, \tag{8}$$

where N_m is the number of available modes in dataset $\mathbf{d}$, e_i and σ_i denotes individual error components (including both natural frequencies and mode shapes error functions) and their respective standard deviations. The term $J(\boldsymbol{\theta}, \mathbf{d})$ is similar to the 'objective function' used in model updating with an optimization approach, which consists of the discrepancy between model-predicted and identified modal properties. It is easy to see that the minimization of $J(\boldsymbol{\theta}, \mathbf{d})$ is equivalently to the maximization of the likelihood function and the posterior PDF (proportional to

the likelihood function as shown in Eq. (2)). Therefore, in this case the optimization approach and Bayesian approach provide the same solution for optimal (for optimization) or MAP (for Bayesian) parameter values, while the Bayesian approach also provides estimation uncertainty of updating parameters as well as model evidence.

In the case that multiple sets of measurements from different tests are available, they can be fused together to provide the joint posterior PDF by assuming all datasets are independent:

$$p(\mathbf{D}\,|\,\boldsymbol{\theta}) = \hat{c}\exp\left(\sum_{n=1}^{N} -\frac{1}{2} J(\boldsymbol{\theta}, \mathbf{d}_n)\right) \tag{9}$$

where $\mathbf{D}$ collects all the datasets $\mathbf{D} = [\mathbf{d}_1 \ ... \ \mathbf{d}_N]$. During the dynamic tests, different modes can be excited and identified each time, therefore, different datasets may contain different modes, or even different number of sensors. However, the fusion of multiple datasets follows the same procedure in Eq. (9). Different MCMC sampling methods can be used to evaluate the posterior PDF such as the Metropolis-Hastings (MH) [46], the adaptive MH [47], or the Transitional MCMC [48].

2.1.2 Phase II: Updating of the nonlinearities

The updating of structural nonlinearity requires the whole NNM curves, as larger amplitude response contains richer information about the nonlinear behavior. Similar error functions for natural frequencies and mode shapes are defined here by considering NNMs at different energy levels:

$$e_{\lambda,j}^{m}(\boldsymbol{\theta}^{nl}) = \tilde{\lambda}_{m,j} - \lambda_{m,j}(\boldsymbol{\theta}^{nl}) + r_m \tag{10}$$

$$\mathbf{e}_{\phi,j}^{m}(\boldsymbol{\theta}^{nl}) = \frac{\tilde{\boldsymbol{\Phi}}_{m,j}}{\left\|\tilde{\boldsymbol{\Phi}}_{m,j}\right\|} - a_{m,j}\frac{\Gamma\boldsymbol{\Phi}_{m,j}(\boldsymbol{\theta}^{nl})}{\left\|\Gamma\boldsymbol{\Phi}_{m,j}(\boldsymbol{\theta}^{nl})\right\|} \tag{11}$$

in which $\boldsymbol{\theta}^{nl}$ denotes the vector of coefficient parameters of the nonlinearity function, and the subscript *j* denotes the vibration amplitudes (energy levels) of the NNMs. r_m refers to the linear natural frequency residual at Phase I and is defined as $r_m = \lambda_m(\hat{\boldsymbol{\theta}}) - \tilde{\lambda}_{m,1}$, where $\hat{\boldsymbol{\theta}}$ denotes the MAP value of $\boldsymbol{\theta}$ and $\tilde{\lambda}_{m,1}$ is the corresponding eigenfrequency of identified NNMs at the smallest amplitude. This term is introduced here to eliminate propagation of errors from the linear model.

The error function terms $e_{\lambda,j}^{m}(\boldsymbol{\theta}^{nl})$ and $\mathbf{e}_{\phi,j}^{m}(\boldsymbol{\theta}^{nl})$ refer to specific points on the NNM curves, and different tests may retain different total number of points on the curves. To account for this imbalance, the error functions in Eqs. (10) and (11) are averaged by the number of points on the NNMs. Therefore, a similar term as Eq. (8) is derived for nonlinear model updating at phase II:

$$J(\boldsymbol{\theta}^{nl}, \mathbf{d}) = \sum_{m=1}^{N_m}\left[\frac{1}{N_p^m}\sum_{j=1}^{N_p^m}\left(\frac{e_{\lambda,j}^{m}(\boldsymbol{\theta}^{nl})}{\sigma_{\lambda_{m,j}}}\right)\right]^2 + \sum_{m=1}^{N_m}\left[\frac{1}{N_p^m}\sum_{j=1}^{N_p^m}\frac{\mathbf{e}_{\phi,j}^{m}(\boldsymbol{\theta}^{nl})^T\mathbf{e}_{\phi,j}^{m}(\boldsymbol{\theta}^{nl})}{\sigma_{\phi_m}^2}\right] \tag{12}$$

where N_p^m denotes the number of points on the m^{th} NNM in each test. $\sigma_{\lambda_{m,j}}$ is defined similar to σ_{λ_m} as $\sigma_{\lambda_{m,j}} = w_m \mathrm{CoV}_\lambda \tilde{\lambda}_{m,j}$ and CoV_λ here is averaged among different energy levels. The fusion of multiple datasets from different tests follow the same procedure as the linear model updating case.

2.2 Bayesian Model Class Selection

One of the important advantages of Bayesian inference for model updating is model class selection to identify the most plausible model. The selection criterion is simply the evidence of model *M* given measurement data $\mathbf{D}$, $p(\mathbf{D} \mid M)$. The evidence term usually lacks an analytical solution, and sampling approaches such as MCMC are often employed to provide numerical estimation, e.g., MH algorithm [49] or TMCMC which provides the evidence as a by-product [48]. In this study, class selection is focused on selecting the most probable nonlinearity function. Linear mode class selection follows exactly the same procedure presented in this section; however, it is not considered herein. The Bayes' theorem is presented below for nonlinear coefficient parameters:

$$p(\boldsymbol{\theta}^{nl} \mid \mathbf{D}, M) = \frac{p(\mathbf{D} \mid \boldsymbol{\theta}^{nl}, M)\, p(\boldsymbol{\theta}^{nl} \mid M)}{p(\mathbf{D} \mid M)} \tag{13}$$

The following is readily available by rearranging the terms:

$$p(\mathbf{D} \mid M) = \frac{p(\mathbf{D} \mid \boldsymbol{\theta}^{nl}, M)\, p(\boldsymbol{\theta}^{nl} \mid M)}{p(\boldsymbol{\theta}^{nl} \mid \mathbf{D}, M)} \tag{14}$$

The only uncertain term on the right is the posterior PDF $p(\boldsymbol{\theta}^{nl} \mid \mathbf{D}, M)$. In the literature, the posterior distribution is often assumed to be a Gaussian distribution, which is usually a good approximation when the parameters are globally identifiable [10]. In the applications of wing-engine structure presented in later sections, the posterior PDF is also observed to resemble a Gaussian distribution. Substituting the posterior PDF with the Gaussian PDF $N\left(\boldsymbol{\theta}^{nl} \mid \boldsymbol{\mu}_{\boldsymbol{\theta}^{nl}}, \boldsymbol{\Sigma}_{\boldsymbol{\theta}^{nl}}\right)$, the following is derived:

$$p(\mathbf{D} \mid M) = \frac{p(\mathbf{D} \mid \boldsymbol{\theta}^{nl}, M)\, p(\boldsymbol{\theta}^{nl} \mid M)}{N(\boldsymbol{\theta}^{nl} \mid \boldsymbol{\mu}_{\boldsymbol{\theta}^{nl}}, \boldsymbol{\Sigma}_{\boldsymbol{\theta}^{nl}})} \tag{15}$$

In Eq. (14), $\boldsymbol{\theta}^{nl}$ can be any value with non-zero posterior PDF. However, the MAP (same as mean value for Gaussian PDF) of parameters $\hat{\boldsymbol{\theta}}^{nl}$ is used in this study. After substituting the likelihood function and prior PDF and taking the logarithm of both sides, the computation of evidence is shown below:

$$\log\left(p(\mathbf{D} \mid M)\right) = \log\left(p(\mathbf{D} \mid \hat{\boldsymbol{\theta}}^{nl}, M)\right) + \log\left(p(\hat{\boldsymbol{\theta}}^{nl} \mid M)\right) - \log\left(N(\hat{\boldsymbol{\theta}}^{nl} \mid \boldsymbol{\mu}_{\boldsymbol{\theta}^{nl}}, \boldsymbol{\Sigma}_{\boldsymbol{\theta}^{nl}})\right) \tag{16}$$

$$\log\left(p(\mathbf{D} \mid \hat{\boldsymbol{\theta}}^{nl}, M)\right) = -\frac{N_{\mathbf{D}}}{2}\log(2\pi) - \sum_{i}^{N_{\mathbf{D}}}\log(\sigma_i) + \sum_{n=1}^{N}\left(-\frac{1}{2}J(\boldsymbol{\theta}, \mathbf{d}_n)\right) \tag{17}$$

where $N_{\mathbf{D}}$ refers to the total number of error function components in the likelihood.

2.3 Probabilistic Prediction of NNMs

After the joint posterior PDF of parameters are estimated, both parameter uncertainty and error function uncertainty can be propagated into probabilistic response predictions. By rearranging the terms in the definition of the error function in Eq. (10), the following frequency prediction of NNMs is obtained:

$$\lambda_{m,j}^{\text{prediction}} = \lambda_{m,j}(\boldsymbol{\theta}^{nl}) + e_{\lambda,j}^{m} - r_m \tag{17}$$

In Eq. (17), both parameters $\boldsymbol{\theta}^{nl}$ and error function $e_{\lambda,j}^{m}$ follow Gaussian distributions $\boldsymbol{\theta}^{nl} \sim N\left(\boldsymbol{\theta}^{nl} \mid \boldsymbol{\mu}_{\boldsymbol{\theta}^{nl}}, \boldsymbol{\Sigma}_{\boldsymbol{\theta}^{nl}}\right)$ and $e_{\lambda,j}^{m} \sim N\left(e_{\lambda,j}^{m} \mid \mathbf{0}, \sigma_{\lambda_{m,j}}^{2}\right)$. Monte Carlo simulations can be performed to obtain adequate number of NNMs simulations by generating independent samples of $\boldsymbol{\theta}^{nl}$ and $e_{\lambda,j}^{m}$, and then response confidence intervals can be produced from these simulations.

3. Application to a Conceptually Simple Wing-engine Structure

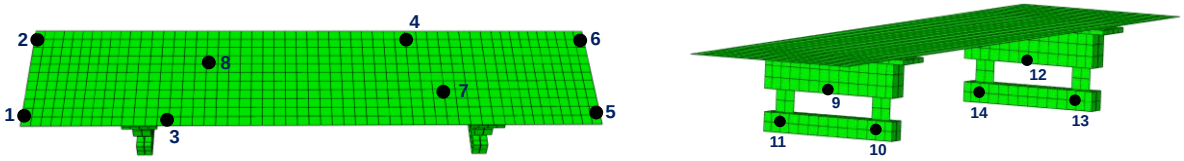
3.1 Structure Description and Instrumentation

The tested structure represents a conceptually simple wing-engine system as shown in Figure 1 [50]. The scaled structure consists of a rectangular aluminum wing plate on the top (size of $1000\ \text{mm} \times 220\ \text{mm}$ and thickness of 6 mm), and two steel pylons (Figure 1(b)). Each of the two pylons have two thin steel plates (referred to as 'springs') which are clamped by two supporting aluminum blocks at the bottom of the wing plate. Nonlinear behavior is observed at the clamping connections of the steel springs due to the curved inner surfaces of the two supporting aluminum blocks, as illustrated in Figure 1(b). The restoring forces of the steel springs are a nonlinear function of the pylon displacement because the effective lengths of the springs change with vibration amplitude, which introduces nonlinear stiffness. The whole structure is hanging by 12 soft springs located at the four corners of the wing plate. The wing-engine structure is instrumented with 14 accelerometers and one single point excitation shaker. Eight accelerometers are mounted on the top of the wing plate measuring vertical acceleration (Figure 2(a)), and three accelerometers are mounted on each of the two pylons measuring horizontal acceleration (Figure 2(b)). The single point shaker is located under the structure with excitation force applied at the same location as sensor 7.



(a) (b)

Figure 1. Wing-engine structure and instrumentation (a) and detailed view of nonlinear connection and modeling assumption (b). Only the left shaker shown in (a) was used for exciting the structure during the experiment.



(a) (b)

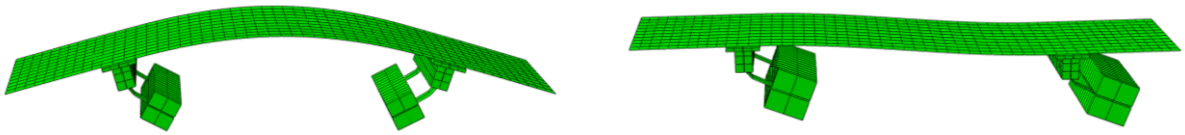
Figure 2. Layout of accelerometers and FE model in Abaqus.

3.2 FE Model and ROM

A linear FE model of the wing-engine structure is created in Abaqus [51]. It includes 639 linear quadrilateral elements of type S4R, and 440 linear hexahedral elements of type C3D8R, and has a total of 6876 DOFs. The discretization of the FE model is selected such that, within the frequency range of interest, the dynamic characteristics of the structure have converged. The local nonlinearities at the connections of the pylons are not considered in this linear model, and the connections of the steel springs with aluminum blocks are assumed to be perfect (Figure 1(b)). The first two mode shapes of the FE model are shown in Figure 3. Significant displacements at the pylons are observed which are influenced by the nonlinearities.

The evaluation of the posterior PDF using MCMC techniques requires large number of computations of NNMs from the numerical model, therefore, it is computationally demanding to directly include nonlinearity in the detailed Abaqus model for this task. A simplified model with less DOFs is needed to include the nonlinearities and reduce the computation burden. The Craig-Bampton method is employed to obtain a ROM of the linear model [52]. All the DOFs associated with the sensor locations are treated as boundary points and the corresponding static constraint modes are retained in the ROM. Only the translational DOFs corresponding to the measured directions are included, i.e., the DOFs in the Z direction for sensors 1 - 8, and the DOFs in the X direction for sensors 9 - 14. To model the nonlinearities at the pylons, nonlinear restoring forces that depend on the relative displacements between corresponding DOFs are added to the ROM, i.e., between sensor 9 - 10, 9 - 11, 12 - 13 and 12 - 14. The ROM is then used to compute theoretical NNMs which are compared with the experimental results for model updating. Note that the two-phase model updating approach proposed here is in principle not restricted to a particular model reduction method and could also work without (albeit at a much higher computational cost).

In this study, the HBM is used to directly compute NNMs for response amplitudes that correspond to the amplitudes measured experimentally. These responses are the only ones required to evaluate the error functions defined in Eqs. (10) and (11). It is worth noting that damping properties do not have to be included in the ROM for the computation of NNMs. Effective damping ratios can be estimated from the measured backbone curves [53] and directly incorporated in the ROM after updating. To include the damping parameters in the model updating, the backbone curves measured experimentally should be compared directly with the backbone curves computed from forced and damped simulations [38] instead of the NNMs.



(a) (b)

Figure 3. Mode 1 (a) and mode 2 (b) of the Abaqus model.

3.3 Experimental Results

The NNMs of the wing-engine structure are identified using CBC through phase resonance testing. CBC is a model-free method that relies on feedback control to explore the dynamic behavior of nonlinear systems directly during experimental tests [54]. CBC has been used to extract important nonlinear dynamic features such as backbone curves [36], nonlinear frequency response curves [55] and limit-point bifurcation curves [56, 57], on a range of harmonically forced mechanical structures, including nonlinear energy harvesters [55, 56], a bilinear oscillator[58] and a nonlinear beam with harmonically coupled modes [57, 59]. To identify backbone curves, CBC adjusts the frequency of excitation such that the response and excitation are in phase quadrature. The evolution of the excitation frequency and structure response is then captured by maintaining quadrature for increasing excitation amplitudes. So far, CBC has been applied to conceptually simple structures with at most a couple of degrees of freedom. In this paper, we show that CBC is applicable to more complex, multi-degree-of-freedom systems.

The backbone curves identified for the first and second modes of the wing-engine structure are shown in Figure 4 and Figure 5, respectively. For conciseness, the structure response is shown only at sensors 9 - 14. The response amplitude at sensors 10, 11, 13 and 14 is observed to be one order of magnitude larger than the response measured at sensors 9 and 12. This is because the former sensors are located at the bottom of pylons (Figure 2(b)).

Figure 4 and Figure 5 show several backbone curves, each of which was obtained by measuring the phase quadrature condition between the excitation and a particular sensor. For the first mode, this leads to 14 different curves - one for every accelerometer on the structure. From a theoretical perspective, different backbone curves represent the same NNM and should therefore overlap each other [38]. However, due to the single-point nature of the applied excitation, the energy provided by the external force is not perfectly distributed across the whole structure and the response of the structure is not monophase. However, the qualitative agreement and the relatively small errors between different backbone curves suggest that phase differences that exist between different sensors are acceptable, and that the NNM of the underlying conservative structure is close to the

identified backbone curves. For mode 2, backbone curves were identified for only 5 sensors. For the other 9 sensors, the quadrature condition could not be reached with the desired accuracy tolerance of 5×10^{-3} rad (or $0.29°$). It is thought that this issue is solely due to the inappropriate distribution of the excitation as no issue with the controller was observed.

When considering all 7 measured harmonics, the response amplitude for the first NNM shows a peak at about 15.3 Hz (Figure 4). This peak is due to the presence of a modal interaction between the first and a higher-frequency mode. Modal interactions usually lead to the presence of loops in the frequency-amplitude curve of the NNM. These loops pose issues for computing the error functions used in model updating (Eqs. (10) and (11)) as the curve can no longer be uniquely parameterized by the frequency or response amplitude, i.e., multiple response amplitudes are possible for a given frequency and multiple frequencies are possible for a given response amplitude. Note that only parts of the loop were measured experimentally, which explains the greater variability observed in the results around the 15.3 Hz peak (Figure 4). Based on the available experimental data, it is not possible to systematically identify which one of those multiple responses has been measured and hence to correctly pair experimental data and model prediction points in the modal interaction region. To overcome this issue in theoretical calculations, modal interactions were filtered out by reducing the number of harmonics used in the HBM to only one. Similarly, only the first harmonic of the responses measured experimentally was used. The differences in response amplitudes resulting from the use of one and seven harmonics are shown in Figure 4 and Figure 5.

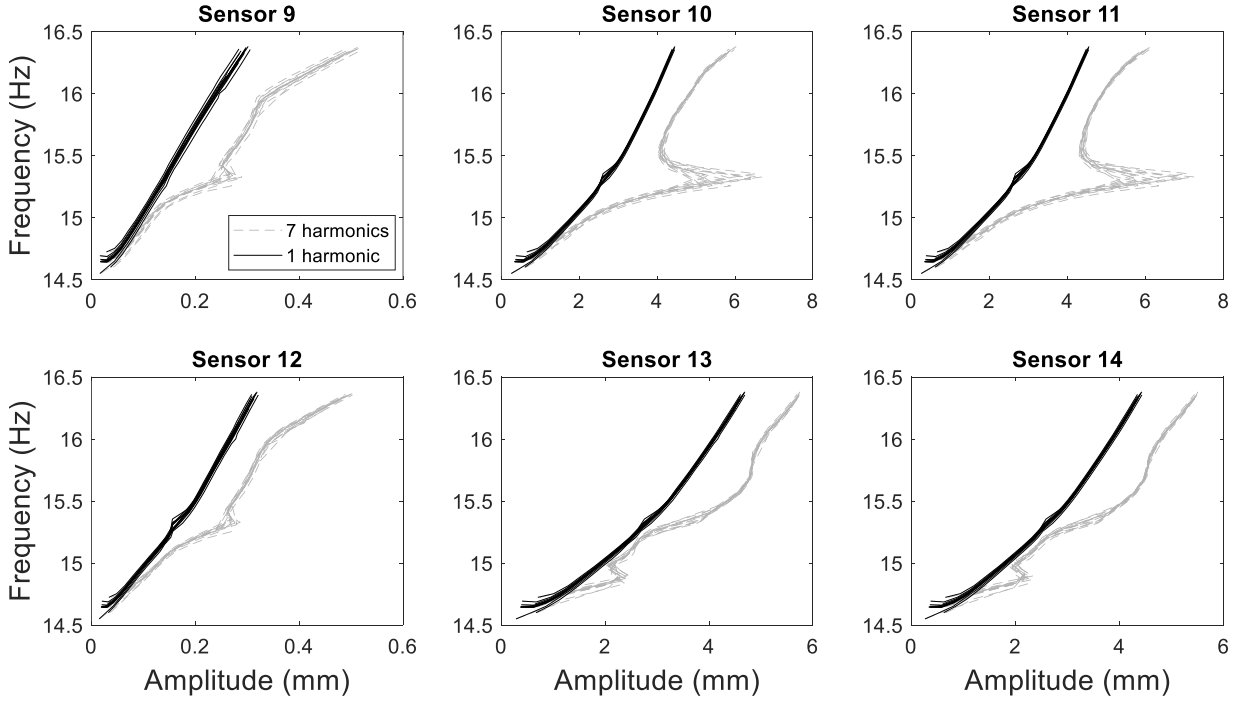


Figure 4. Identified backbones of NNM 1.

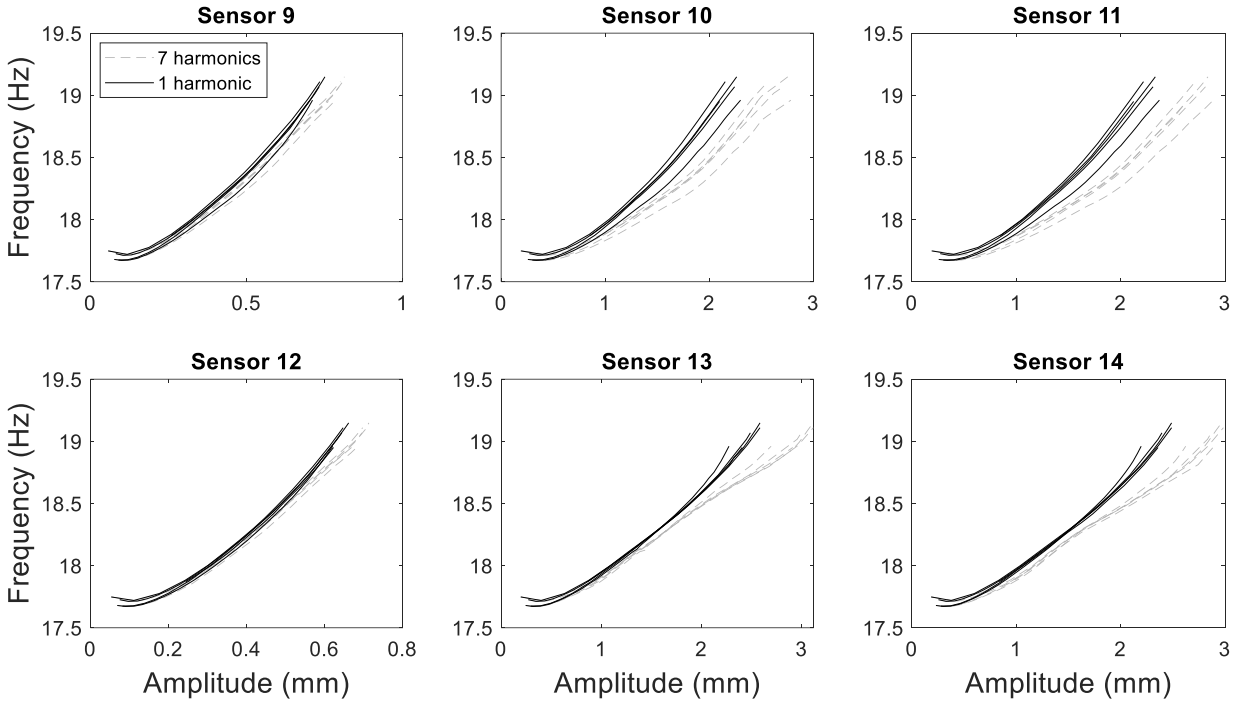


Figure 5. Identified backbones of NNM 2.

4. Model Updating Results

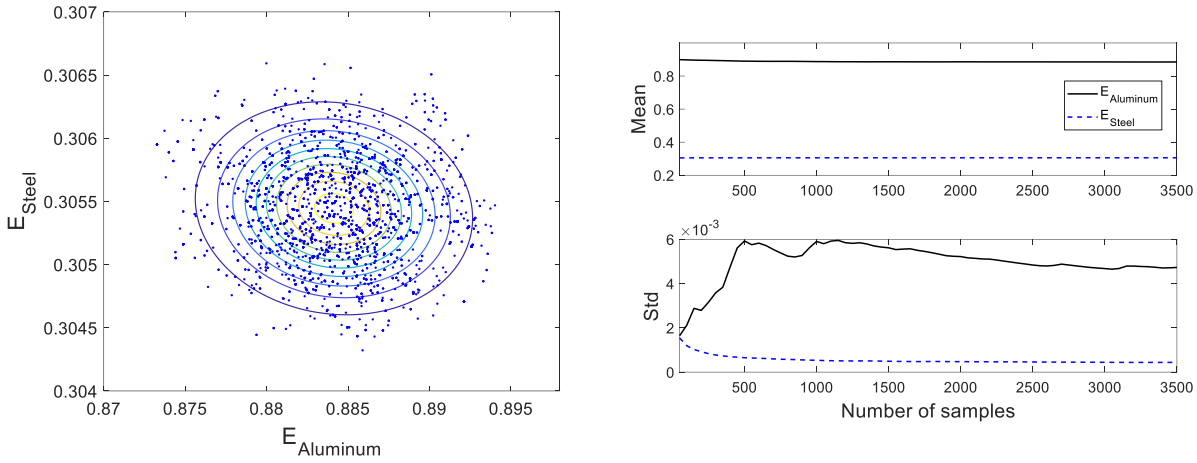
4.1 Linear Model Updating Results

The wing-engine structure is made of two materials: aluminum and steel. The Young's modulus of these two materials are chosen as the linear updating parameters, i.e., $\boldsymbol{\theta} = \left[E_{\text{Aluminum}} \quad E_{\text{Steel}} \right]^T$. The values of updating parameters are normalized to their initial values: $E_{\text{Aluminum}}^{\text{Initial}} = 68.9$ GPa and $E_{\text{Steel}}^{\text{Initial}} = 200$ GPa. The proposed Bayesian updating framework is implemented to update the selected Young's modulus based on the linear modes which are estimated as the identified NNMs 1 and 2 at their lowest energy levels. Therefore, 14 sets of mode 1 and 5 sets of mode 2 are used in the updating process. MH algorithm is used to generate 3500 samples of the joint posterior PDF, and then the first 500 samples are removed as burning-in strategy to eliminate the effects of transitional samples. The sample acceptance rate is adjusted to be in the range recommended in [60]. The evolution histories of sample mean and standard deviation are shown in Figure 6(b). It can be seen that the sample mean and standard deviation have converged and 3500 samples are sufficient for evaluating the posterior PDF. The sample distribution after burning-in is shown in Figure 6(a). The contour plots are from a Gaussian distribution with its mean and covariance the same as the sample statistics. It is seen that the sample scatter follows the Gaussian contours well, implying that the posterior PDF resembles the Gaussian distribution.

The sample mean and standard deviation are reported in

Table 1. It is observed that E_{Steel} has been reduced significantly (around 70%) in the updating process. This large reduction is attributed to an error in the modeling of the boundary conditions of the springs which are the only components made out of steel. In reality, the inner surfaces of the aluminum blocks are curved to introduce the nonlinear restoring force (Figure 1(b)). However, the linear FE model assumes that the aluminum blocks are straight and that the clamping is perfect (Figure 1(b)). As a result, the length of the steel springs is underestimated. In the model updating, the Young's modulus of steel is drastically reduced to compensate for this modeling error. The modal properties of the calibrated model match the identified counterparts very well (see Table 2). A validated model with more accurate representation of the geometry would overcome the modeling error. Note that the modeling error cannot be corrected by the large reduction of parameter value but is compensated to provide accurate modal properties in this study. The current Abaqus model is created based on the best knowledge of the authors as the portions of the aluminum blocks that are in contact with the steel springs are not precisely known and appear to be different at the front and at the back of the pylons. The mesh size of the steel springs has been verified to have converged and has negligible effects on the model updating. A good tutorial about model updating process and modeling errors can be found in [61]. Another possible reason is that the initial Young's modulus of steel and aluminum are overestimated compared to their true values since the precise material compositions of the structure are not available.

The estimated standard deviations of the parameters are very small indicating negligible uncertainty in the underlying linear system. Therefore, the ROM of the linear model is generated only based on the MAP values of the updating parameters. The natural frequencies and mode shapes of the linear model before and after updating are compared with their identified counterparts in Table 2. The post-updating values are from the FE model using the MAP values of parameters and are much closer to the identified values. The identified natural frequencies are reported as the mean values over several tests. The modal assurance criteria (MAC) values are computed between model-predicted and identified mode shapes and the mean values for different tests are reported in Table 2. It is observed that the MAC values are also improved significantly after model updating, especially for mode 1.



(a) (b)

Figure 6. (a) MH samples of linear model updating and contour plot of approximated Gaussian distribution; (b) evolution time histories of sample mean and standard deviation.

Table 1. Sample mean and standard deviation of linear model updating.

	E_{Aluminum}	E_{Steel}
Mean	0.88	0.31
Std ($\times 10^{-3}$)	3.93	0.39

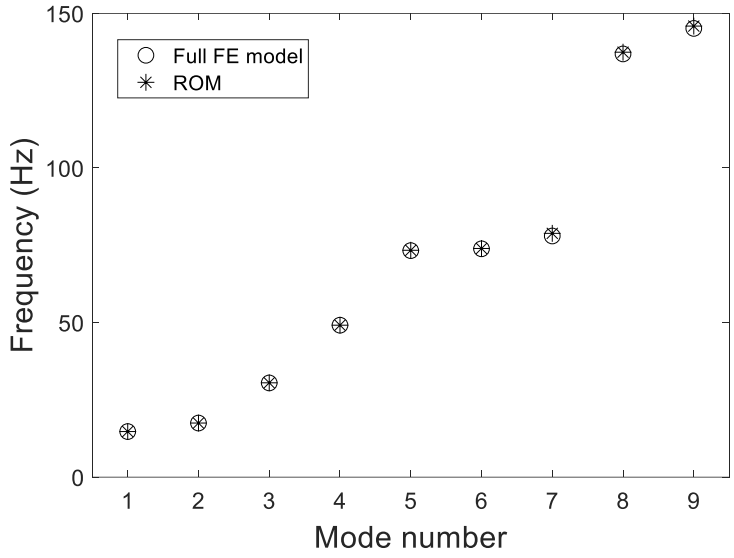
Table 2. Linear modes comparison before and after linear model updating.

	Frequency (Hz)			MAC	
	Initial	Updated	Identified	Initial	Updated
Mode 1	22.78	14.75	14.65	0.788	0.999
Mode 2	30.91	17.50	17.71	0.968	0.985

4.2 Nonlinear Model Updating and Model Class Selection

As mentioned before, the estimated parameter uncertainty in the linear model is negligible and thus the ROM is generated only based on the MAP values of the linear parameters. The first 15 internal mode shapes of the linear model (6 rigid-body-like modes caused by the hanging springs and the first 9 vibration modes) and 14 static constraint modes associated with the measured DOFs are retained in the ROM which comprises a total of 29 DOFs. The natural frequencies of the ROM are compared with those of the full model in Figure 7(a), and the relative frequency errors and MAC values of the corresponding mode shapes are shown in Figure 7(b). The ROM agrees very well with the full model for the first 9 modes. However, the accuracy of the ROM deteriorates

significantly for higher modes (>9) since they are not included in the Craig-Bampton model reduction.



(a)

Mode	Relative frequency error (%)	MAC
1	0.00	1.000
2	0.00	1.000
3	0.13	1.000
4	0.02	1.000
5	0.15	1.000
6	0.15	1.000
7	1.09	1.000
8	0.41	0.990
9	0.52	0.956

(b)

Figure 7. Natural frequency comparison between full FE model and ROM (a) and relative frequency errors and MAC (b).

The nonlinearity identification process usually consists of three steps: (1) localization, (2) characterization and (3) parameter identification. The localization step is trivial given that the nonlinearities were implemented deliberately. The characterization step requires identifying the optimal functional form describing the nonlinearities, and parameter identification entails estimating coefficient parameters. Steps (2) and (3) are here jointly carried out through a Bayesian model class selection and updating process. In this study, five model classes with different nonlinear functions are considered to represent the nonlinear force-displacement relationship of the pylon connections. The considered functions are all polynomials as the analysis of the experimental data collected for sine sweep excitation around the first two modes shows that the nonlinearity is smooth. The five nonlinear functions considered are summarized in Table 3. The five nonlinearity forms in Table 3 are selected after an extensive screening process of reasonable polynomial functions, where different orders of polynomials, and combinations of them have been investigated. The selected five nonlinearities provide the most reasonable NNM predictions compared to the measurements with relatively simple polynomial forms. More polynomials can be included in the functions, but it is found that additional higher order polynomials are not providing meaningful improvements on NNM predictions. Only odd functions are selected in this study because the measured backbone curves only show hardening effect as observed in Figures 4 and 5, and no softening effect exists. The authors have examined the performance of even nonlinearity functions in the first stage of screening candidate functions, but they are eventually excluded. It is worth noting that asymmetrical effects of the backbones were observed in earlier studies on the structure [62, 63], however, the structure was modified since then, especially the steel springs clamping connection. The nonlinearity is found to be sensitive to the connection conditions. Based on the measured backbones in this study, the nonlinearity has changed and is

different from previous observations. A static test on the studied wing-engine structure was performed by Delli Carri et al. [50] and showed that the nonlinear form was an odd polynomial function, which is consistent with this study. Cubic splines could have been considered to provide more flexibility to our model [34]; however, this was considered outside the scope of this work. The coefficients c_i^j denotes the updating parameters in each model class, with one updating coefficient for classes 1 - 3, and two updating coefficients for classes 4 and 5. These updating parameters have been normalized to their initial values in each class (e.g., 0.216 in class 1), which are determined through a preliminary trial and error tuning process to provide a reasonable starting point for the updating process. This process is not required but is recommended as otherwise more samples are needed for MCMC to converge to higher probability area. The nonlinearities at the four locations are assumed to be the same as no obvious difference is observed in the identified NNMs at these locations (Figure 4 and Figure 5). The authors have verified that introducing different nonlinearities at two pylons does not improve the model updating results but increases the number of updating parameters and computation efforts significantly.

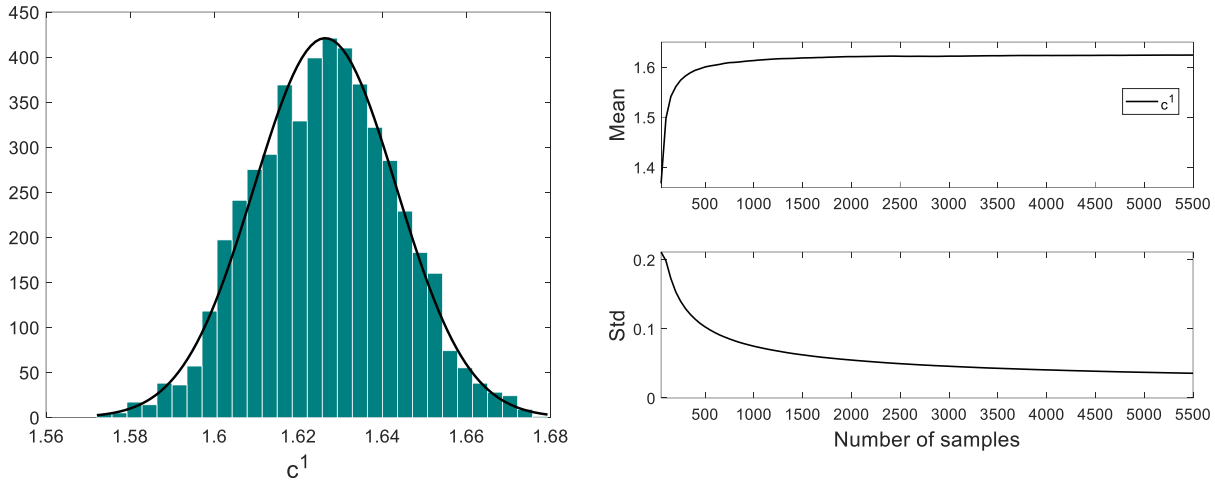
The proposed Bayesian model updating approach is applied to estimate the posterior PDF of the coefficient parameters and the evidence of each model class. The prior distributions of all parameters are assumed to be uniform but with different ranges, i.e., $U(0,\ 10)$ is assumed for classes 1 - 3 (c^1, c^2 and c^3) and the first polynomial coefficient in classes 4 - 5 (c_1^4 and c_1^5), and $U(-10,\ 10)$ is assumed for the second coefficient in classes 4 - 5 (c_2^4 and c_2^5). These assumptions are made to represent lack of prior knowledge about these parameters, especially for parameters c_2^4 and c_2^5. The first coefficient is constrained to be positive as a hardening effect is observed from the identified backbones. A total of 5500 samples of the posterior PDF are generated using the MH algorithm, with the first 500 burned in. The evolution of sample mean and standard deviation for model class 1 are plotted in Figure 8(b) showing the convergence of these statistics, which verifies that the current number of samples is adequate. The sample histograms for classes 1 - 3, and sample distribution for classes 4 - 5 are shown in Figure 8 - 10. The PDF (classes 1 - 3) and contour lines of the approximated Gaussian distribution (classes 4 - 5) are also shown, with their means and covariances computed from the samples. The Gaussian PDFs in Figure 8 - 9 have been normalized to have peak values the same as the highest bins of histograms. It is seen that for all model classes the samples generally follow the approximated Gaussian distribution, which verifies the Gaussian assumption in the proposed evidence computation in section 2.2. Strong correlations between c_1^4 and c_2^4, as well as c_1^5 and c_2^5, are observed from Figure 10(a) and (b), which is caused by their compensation effects since c_2^4 and c_2^5 have negative signs. The sample mean and standard deviation for all classes are reported in Table 4. It is seen that the estimated parameter uncertainties for classes 1 - 3 are similar, while classes 4 - 5 have significantly larger uncertainties, especially for parameters c_2^4 and c_2^5 which represent the high order polynomial terms. The strong compensation effects between the first positive cubic terms (c_1^4 and c_1^5) and the second negative terms (c_2^4 and c_2^5) can be the cause of the large parameter uncertainties. The significant

uncertainties in c_2^4 and c_2^5 suggest their low sensitivities to the NNMs, which implies that they can be redundant in the nonlinearity function. This is verified by model class selection results presented below.

The value of evidence for each of the five considered model classes is computed using the proposed evidence estimation approach and reported in the last column of Table 3. It can be seen that class 2 has the largest evidence value, while classes 4 and 5 have comparable but slightly smaller evidence, and classes 1 and 3 have much smaller values. Compared to class 2 with only cubic polynomial, classes 4 and 5 also include higher order terms, therefore, they have more flexibility in their nonlinearities than class 2 (i.e., the likelihood functions of classes 4 and 5 are larger or equal to that of class 2). However, the inclusion of extra parameters (c_2^4 and c_2^5) reduces the value of prior PDF $\log\left(p(\hat{\boldsymbol{\theta}}^c \mid M)\right)$ in Eq. (15). According to the assumed uniform distributions, $p(\hat{\boldsymbol{\theta}}^c \mid M_2) = 1/10$ while $p(\hat{\boldsymbol{\theta}}^c \mid M_4) = p(\hat{\boldsymbol{\theta}}^c \mid M_5) = 1/200$. The prior distribution here is similar to the Occam's razor, as it assigns penalty to extra parameters. The Bayesian class selection will choose the model with less complexity (smaller number of parameters) unless the improvement from addition of extra parameters outweighs the penalty (from prior distribution). In this study, higher order polynomials are not considered as they have lower evidence. Therefore, Bayesian class selection algorithm automatically enforces the principle of parsimonious model with the largest prediction capability.

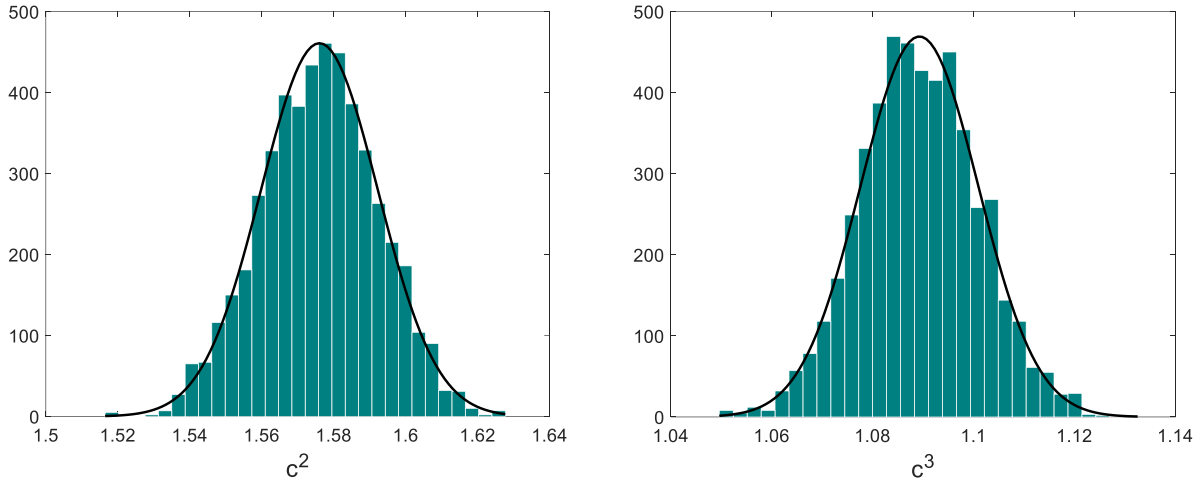
Table 3. Model classes of nonlinearity function and the estimated evidence.

Model classes	Nonlinearity function	Evidence: $\log\left(p(\mathbf{D} \mid M)\right)$
Class 1	$f_{nl}(x) = c^1 \times 0.216\,\text{sign}(x)x^2$	452.9
Class 2	$f_{nl}(x) = c^2 \times 0.068x^3$	619.2
Class 3	$f_{nl}(x) = c^3 \times 0.03\,\text{sign}(x)x^4$	476.8
Class 4	$f_{nl}(x) = c_1^4 \times 0.0884x^3 - c_2^4 \times 0.0027\,\text{sign}(x)x^4$	617.2
Class 5	$f_{nl}(x) = c_1^5 \times 0.0748x^3 - c_2^5 \times 0.00084x^5$	617.1



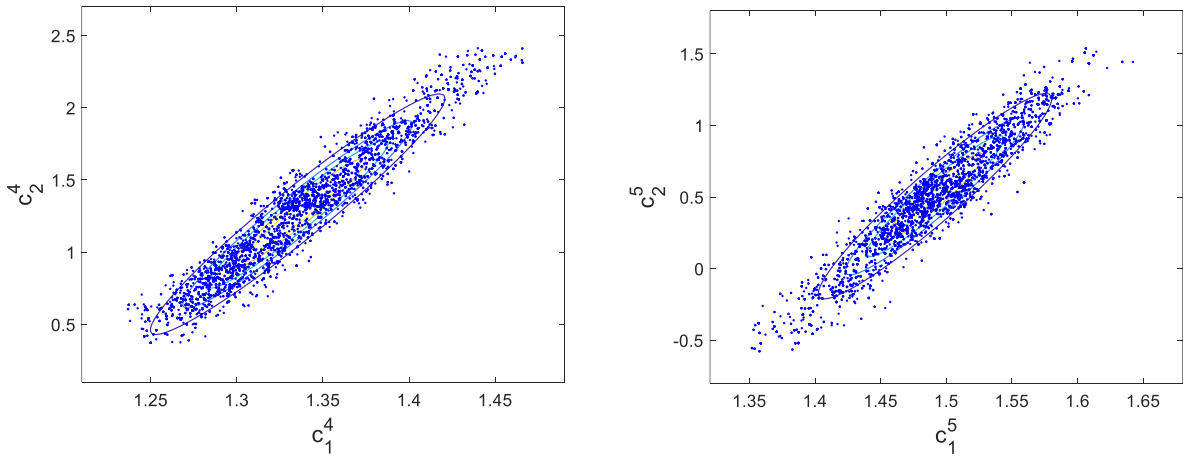
(a) (b)

Figure 8. (a) Sample histograms and approximated Gaussian PDF of model classes 1; (b) Evolution histories of sample mean and standard deviation.



(a) (b)

Figure 9. Sample histograms and approximated Gaussian PDFs of model classes 2 (a) and 3 (b).



(a) (b)

Figure 10. Sample distribution and contour plots of approximated Gaussian PDFs of model classes 4 (a) and 5 (b).

Table 4. Sample mean and standard deviation of nonlinear model updating.

Model classes	Parameters	Mean	Std
Class 1	c^1	1.63	0.017
Class 2	c^2	1.58	0.016
Class 3	c^3	1.09	0.012
Class 4	c_1^4, c_2^4	1.34, 1.26	0.046, 0.443
Class 5	c_1^5, c_2^5	1.49, 0.51	0.049, 0.391

4.3 Bayesian Prediction of NNMs

Model class 2 is selected as the best model in the view of identified NNMs because of its largest evidence. This model is used for probabilistic NNM predictions using the proposed approach in section 2.3. The parameter uncertainty (assumed to have Gaussian distribution) and the error function uncertainty (assumed to have zero-mean Gaussian distribution with standard deviation estimated from the identified NNMs) are propagated into the predictions. A total of 200 Monte Carlo simulations are performed using independent samples from the posterior PDF and the error function distribution. Then a 95% quantile interval is generated by sorting the 200 model-predicted NNMs at different amplitudes and then selecting the 6^{th} and 195^{th} sorted values as the lower and upper bounds. The estimated quantile intervals and the identified NNMs are shown in Figure 11 and Figure 12. It can be seen that the identified NNMs generally fall within the estimated confidence intervals. Furthermore, intervals of mode 2 have larger bounds than that of mode 1 due to the larger standard deviation of error function for mode 2 (the identified NNM 2 has greater variability shown in Figure 5). The identified backbones of mode 1 at sensors 9 and 13 slightly fall out of the confidence bounds, due to modeling errors and NNMs identification error.

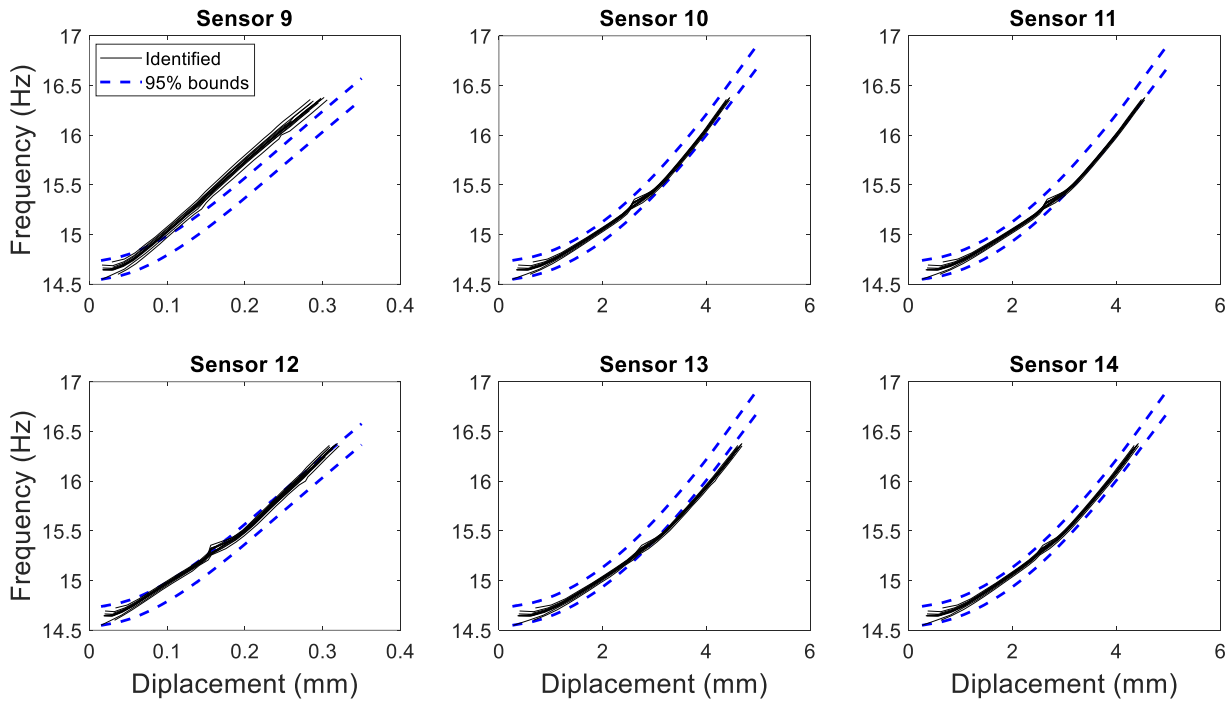


Figure 11. Confidence intervals of NNM 1 and the identified counterparts.

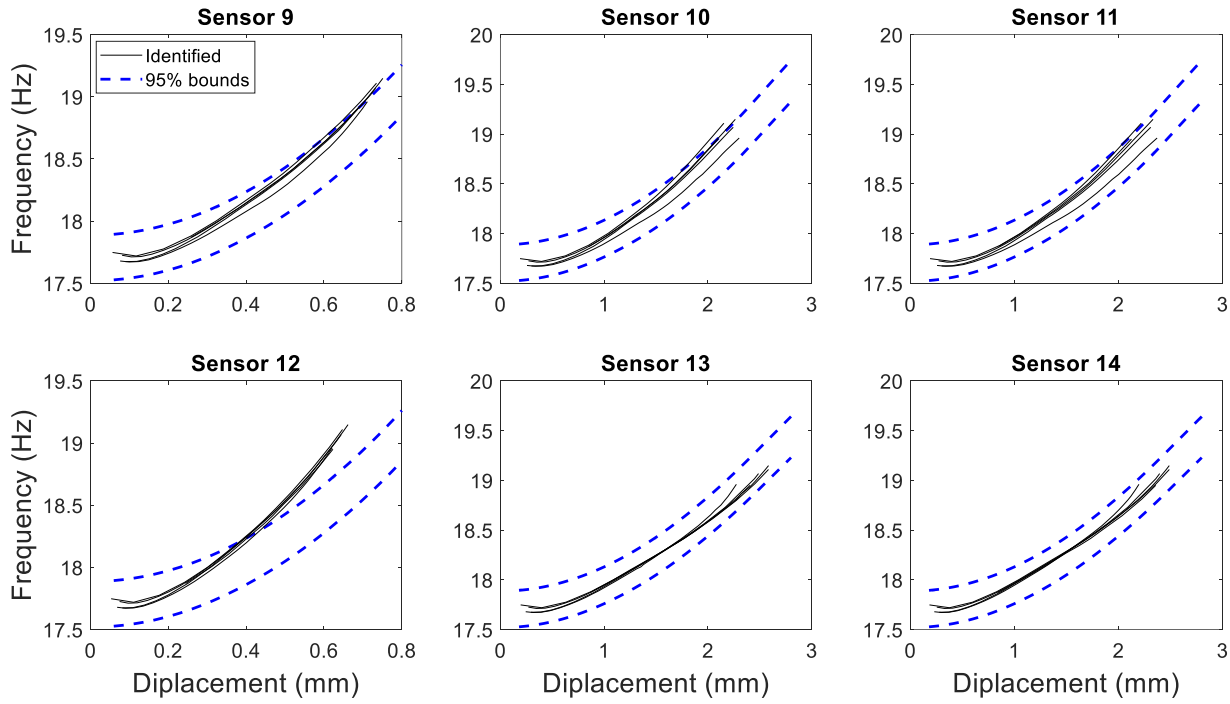


Figure 12. Confidence intervals of NNM 2 and the identified counterparts.

5. Conclusions

This paper presents a two-phase Bayesian model updating and class selection of nonlinear structures using experimentally identified NNMs. The proposed method is applied to a conceptually simple wing-engine system with nonlinear connections. Two NNMs of the system are identified using CBC for phase resonance testing. At phase I, the linear FE model is updated to represent the underlying linear system of the structure using NNMs at the lowest energy level. Then a ROM is generated from the updated FE model using the MAP values of the parameters. The linear model uncertainty is not considered because the parameter uncertainty is negligible. At phase II, the ROM is combined with nonlinearity functions to represent the nonlinear connections. Five model classes with different polynomial functions are considered, and the proposed Bayesian nonlinear model updating is performed to estimate the posterior PDF and evidence for each model class. The Bayesian class selection approach automatically enforces the principle of parsimonious model and rejects classes 4 and 5 although they have higher order polynomial terms. The model class 2 with a cubic nonlinearity is selected as the most plausible model and is used to perform probabilistic prediction of NNMs by propagating the estimated parameter uncertainty and error function uncertainty. The identified NNMs generally fall within the 95% confidence interval of predictions.

The application considered demonstrates the effectiveness of the proposed Bayesian model updating and class selection methodology for nonlinear structures which are assumed to exhibit elastic deformations and to return to the same unique equilibrium position when at rest. Behaviors like buckling, wear, tear, and material nonlinearity are not considered. The proposed method is particularly appropriate for structures with localized stiffness nonlinearities that manifest themselves for sufficiently large vibration amplitudes. The proposed method also has the potential to be applied to structures where nonlinear effects occur for small vibration amplitudes (such as with friction) if phase I of the model updating is modified to include and to estimate the parameters of those nonlinearities.

Data Statement

Experimental data collected in this study are available at [*DOI to be inserted at proofing*].

Acknowledgements

The authors acknowledge partial support of this study by the National Science Foundation Grant number 1903972. L. Renson acknowledges the financial support of the Royal Academy of Engineering, Research Fellowship #RF1516/15/11. The opinions, findings, and conclusions expressed in this paper are those of the authors and do not necessarily represent the views of the sponsors and organizations involved in this project.

References

1. Friswell, M. and J.E. Mottershead, *Finite element model updating in structural dynamics*. Vol. 38. 2013: Springer Science & Business Media.

2. Zhang, Q., T.-Y.P. Chang, and C.C. Chang, *Finite-element model updating for the Kap Shui Mun cable-stayed bridge.* Journal of Bridge Engineering, 2001. **6**(4): p. 285-293.
3. Brownjohn, J.M.W., P. Moyo, P. Omenzetter, and Y. Lu, *Assessment of highway bridge upgrading by dynamic testing and finite-element model updating.* Journal of Bridge Engineering, 2003. **8**(3): p. 162-172.
4. Teughels, A. and G. De Roeck, *Structural damage identification of the highway bridge Z24 by FE model updating.* Journal of Sound and Vibration, 2004. **278**(3): p. 589-610.
5. Jaishi, B., H.-J. Kim, M.K. Kim, W.-X. Ren, and S.-H. Lee, *Finite element model updating of concrete-filled steel tubular arch bridge under operational condition using modal flexibility.* Mechanical Systems and Signal Processing, 2007. **21**(6): p. 2406-2426.
6. Reynders, E., G.D. Roeck, P. Gundes Bakir, and C. Sauvage, *Damage identification on the Tilff Bridge by vibration monitoring using optical fiber strain sensors.* Journal of engineering mechanics, 2007. **133**(2): p. 185-193.
7. Fang, S.-E., R. Perera, and G. De Roeck, *Damage identification of a reinforced concrete frame by finite element model updating using damage parameterization*. Journal of Sound and Vibration, 2008. **313**(3-5): p. 544-559.
8. Moaveni, B., A. Stavridis, G. Lombaert, J.P. Conte, and P.B. Shing, *Finite-element model updating for assessment of progressive damage in a 3-story infilled RC frame.* Journal of Structural Engineering, 2012. **139**(10): p. 1665-1674.
9. Song, M., S. Yousefianmoghadam, M.-E. Mohammadi, B. Moaveni, A. Stavridis, and R.L. Wood, *An application of finite element model updating for damage assessment of a two-story reinforced concrete building and comparison with lidar.* Structural Health Monitoring, 2018. **17**(5): p. 1129-1150.
10. Beck, J.L. and L.S. Katafygiotis, *Updating models and their uncertainties. I: Bayesian statistical framework.* Journal of Engineering Mechanics, 1998. **124**(4): p. 455-461.
11. Yuen, K.V., J.L. Beck, and S.K. Au, *Structural damage detection and assessment by adaptive Markov chain Monte Carlo simulation.* Structural Control and Health Monitoring, 2004. **11**(4): p. 327-347.
12. Ching, J. and J.L. Beck, *New Bayesian model updating algorithm applied to a structural health monitoring benchmark.* Structural Health Monitoring, 2004. **3**(4): p. 313-332.
13. Muto, M. and J.L. Beck, *Bayesian updating and model class selection for hysteretic structural models using stochastic simulation.* Journal of Vibration and Control, 2008. **14**(1-2): p. 7-34.
14. Simoen, E., G. De Roeck, and G. Lombaert, *Dealing with uncertainty in model updating for damage assessment: A review.* Mechanical Systems and Signal Processing, 2015. **56**: p. 123-149.
15. Sevieri, G., M. Andreini, A. De Falco, and H.G. Matthies, *Concrete gravity dams model parameters updating using static measurements.* Engineering Structures, 2019. **196**: p. 109231.
16. Ntotsios, E., C. Papadimitriou, P. Panetsos, G. Karaiskos, K. Perros, and P.C. Perdikaris, *Bridge health monitoring system based on vibration measurements.* Bulletin of Earthquake Engineering, 2009. **7**(2): p. 469.
17. Lam, H.-F., J. Yang, and S.-K. Au, *Bayesian model updating of a coupled-slab system using field test data utilizing an enhanced Markov chain Monte Carlo simulation algorithm.* Engineering Structures, 2015. **102**: p. 144-155.

18. Behmanesh, I. and B. Moaveni, *Probabilistic identification of simulated damage on the Dowling Hall footbridge through Bayesian finite element model updating.* Structural Control and Health Monitoring, 2015. **22**(3): p. 463-483.
19. Behmanesh, I. and B. Moaveni, *Accounting for environmental variability, modeling errors, and parameter estimation uncertainties in structural identification.* Journal of Sound and Vibration, 2016. **374**: p. 92-110.
20. Sedehi, O., C. Papadimitriou, and L.S. Katafygiotis, *Probabilistic hierarchical Bayesian framework for time-domain model updating and robust predictions.* Mechanical Systems and Signal Processing, 2019. **123**: p. 648-673.
21. Song, M., B. Moaveni, C. Papadimitriou, and A. Stavridis, *Accounting for amplitude of excitation in model updating through a hierarchical Bayesian approach: Application to a two-story reinforced concrete building.* Mechanical Systems and Signal Processing, 2019. **123**: p. 68-83.
22. Song, M., I. Behmanesh, B. Moaveni, and C. Papadimitriou, *Accounting for Modeling Errors and Inherent Structural Variability through a Hierarchical Bayesian Model Updating Approach: An Overview.* Sensors, 2020. **20**(14): p. 3874.
23. Asgarieh, E., B. Moaveni, and A. Stavridis, *Nonlinear finite element model updating of an infilled frame based on identified time-varying modal parameters during an earthquake.* Journal of Sound and Vibration, 2014. **333**(23): p. 6057-6073.
24. Asgarieh, E., B. Moaveni, A.R. Barbosa, and E. Chatzi, *Nonlinear model calibration of a shear wall building using time and frequency data features.* Mechanical Systems and Signal Processing, 2017. **85**: p. 236-251.
25. Chatzi, E.N. and A.W. Smyth, *The unscented Kalman filter and particle filter methods for nonlinear structural system identification with non-collocated heterogeneous sensing.* Structural Control and Health Monitoring: The Official Journal of the International Association for Structural Control and Monitoring and of the European Association for the Control of Structures, 2009. **16**(1): p. 99-123.
26. Astroza, R. and A. Alessandri, *Effects of model uncertainty in nonlinear structural finite element model updating by numerical simulation of building structures.* Structural Control and Health Monitoring, 2019. **26**(3): p. e2297.
27. Song, M., R. Astroza, H. Ebrahimian, B. Moaveni, and C. Papadimitriou, *Adaptive Kalman filters for nonlinear finite element model updating.* Mechanical Systems and Signal Processing, 2020. **143**: p. 106837.
28. Vakakis, A., *Non-linear normal modes (NNMs) and their applications in vibration theory: an overview.* 1997.
29. Kerschen, G., M. Peeters, J.-C. Golinval, and A.F. Vakakis, *Nonlinear normal modes, Part I: A useful framework for the structural dynamicist.* Mechanical systems and signal processing, 2009. **23**(1): p. 170-194.
30. Rosenberg, R., *The normal modes of nonlinear n-degree-of-freedom systems.* 1962.
31. Avramov, K.V. and Y.V. Mikhlin, *Review of applications of nonlinear normal modes for vibrating mechanical systems.* Applied Mechanics Reviews, 2013. **65**(2).
32. Kuether, R.J., L. Renson, T. Detroux, C. Grappasonni, G. Kerschen, and M.S. Allen, *Nonlinear normal modes, modal interactions and isolated resonance curves.* Journal of Sound and Vibration, 2015. **351**: p. 299-310.

33. Renson, L., J.-P. Noël, and G. Kerschen, *Complex dynamics of a nonlinear aerospace structure: numerical continuation and normal modes.* Nonlinear Dynamics, 2015. **79**(2): p. 1293-1309.
34. Noël, J.-P., L. Renson, C. Grappasonni, and G. Kerschen, *Identification of nonlinear normal modes of engineering structures under broadband forcing.* Mechanical Systems and Signal Processing, 2016. **74**: p. 95-110.
35. Peeters, M., G. Kerschen, and J.-C. Golinval, *Modal testing of nonlinear vibrating structures based on nonlinear normal modes: Experimental demonstration.* Mechanical Systems and Signal Processing, 2011. **25**(4): p. 1227-1247.
36. Renson, L., A. Gonzalez-Buelga, D. Barton, and S. Neild, *Robust identification of backbone curves using control-based continuation.* Journal of Sound and Vibration, 2016. **367**: p. 145-158.
37. Peter, S. and R.I. Leine, *Excitation power quantities in phase resonance testing of nonlinear systems with phase-locked-loop excitation.* Mechanical Systems and Signal Processing, 2017. **96**: p. 139-158.
38. Renson, L., T. Hill, D. Ehrhardt, D. Barton, and S. Neild, *Force appropriation of nonlinear structures.* Proceedings of the Royal Society A: Mathematical, Physical and Engineering Sciences, 2018. **474**(2214): p. 20170880.
39. Detroux, T., L. Renson, L. Masset, and G. Kerschen, *The harmonic balance method for bifurcation analysis of large-scale nonlinear mechanical systems.* Computer Methods in Applied Mechanics and Engineering, 2015. **296**: p. 18-38.
40. Renson, L., G. Kerschen, and B. Cochelin, *Numerical computation of nonlinear normal modes in mechanical engineering.* Journal of Sound and Vibration, 2016. **364**: p. 177-206.
41. Peter, S., A. Grundler, P. Reuss, L. Gaul, and R.I. Leine, *Towards finite element model updating based on nonlinear normal modes*, in *Nonlinear Dynamics, Volume 1*. 2016, Springer. p. 209-217.
42. Hill, T., P. Green, A. Cammarano, and S. Neild, *Fast Bayesian identification of a class of elastic weakly nonlinear systems using backbone curves.* Journal of Sound and Vibration, 2016. **360**: p. 156-170.
43. Song, M., L. Renson, J.P. Noël, B. Moaveni, and G. Kerschen, *Bayesian model updating of nonlinear systems using nonlinear normal modes.* Structural Control and Health Monitoring, 2018: p. e2258.
44. Grappasonni, C., J.-P. Noël, and G. Kerschen, *Subspace and nonlinear-normal-modes-based identification of a beam with softening-hardening behaviour*, in *Nonlinear Dynamics, Volume 2*. 2014, Springer. p. 55-68.
45. Kerschen, G., K. Worden, A.F. Vakakis, and J.-C. Golinval, *Past, present and future of nonlinear system identification in structural dynamics.* Mechanical systems and signal processing, 2006. **20**(3): p. 505-592.
46. Hastings, W.K., *Monte Carlo sampling methods using Markov chains and their applications.* 1970.
47. Haario, H., E. Saksman, and J. Tamminen, *An adaptive Metropolis algorithm.* Bernoulli, 2001. **7**(2): p. 223-242.
48. Ching, J. and Y.-C. Chen, *Transitional Markov chain Monte Carlo method for Bayesian model updating, model class selection, and model averaging.* Journal of engineering mechanics, 2007. **133**(7): p. 816-832.

49. Chib, S. and I. Jeliazkov, *Marginal likelihood from the Metropolis–Hastings output.* Journal of the American Statistical Association, 2001. **96**(453): p. 270-281.
50. delli Carri, A., B. Weekes, D. Di Maio, and D. Ewins, *Extending modal testing technology for model validation of engineering structures with sparse nonlinearities: A first case study*. Mechanical Systems and Signal Processing, 2017. **84**: p. 97-115.
51. *Abaqus 6.14*. Dassault Systemes.
52. Craig Jr, R.R. and M.C. Bampton, *Coupling of substructures for dynamic analyses.* AIAA journal, 1968. **6**(7): p. 1313-1319.
53. Peter, S., M. Scheel, M. Krack, and R.I. Leine, *Synthesis of nonlinear frequency responses with experimentally extracted nonlinear modes.* Mechanical Systems and Signal Processing, 2018. **101**: p. 498-515.
54. Sieber, J. and B. Krauskopf, *Control based bifurcation analysis for experiments.* Nonlinear Dynamics, 2008. **51**(3): p. 365-377.
55. Barton, D.A., B.P. Mann, and S.G. Burrow, *Control-based continuation for investigating nonlinear experiments.* Journal of Vibration and Control, 2012. **18**(4): p. 509-520.
56. Renson, L., D.A. Barton, and S.A. Neild, *Experimental tracking of limit-point bifurcations and backbone curves using control-based continuation.* International Journal of Bifurcation and Chaos, 2017. **27**(01): p. 1730002.
57. Renson, L., J. Sieber, D. Barton, A. Shaw, and S. Neild, *Numerical continuation in nonlinear experiments using local Gaussian process regression.* Nonlinear Dynamics, 2019. **98**(4): p. 2811-2826.
58. Bureau, E., F. Schilder, I.F. Santos, J.J. Thomsen, and J. Starke, *Experimental bifurcation analysis of an impact oscillator—tuning a non-invasive control scheme.* Journal of Sound and Vibration, 2013. **332**(22): p. 5883-5897.
59. Renson, L., A. Shaw, D. Barton, and S. Neild, *Application of control-based continuation to a nonlinear structure with harmonically coupled modes.* Mechanical Systems and Signal Processing, 2019. **120**: p. 449-464.
60. Roberts, G.O. and J.S. Rosenthal, *Optimal scaling for various Metropolis-Hastings algorithms.* Statistical science, 2001. **16**(4): p. 351-367.
61. Mottershead, J.E., M. Link, and M.I. Friswell, *The sensitivity method in finite element model updating: A tutorial.* Mechanical systems and signal processing, 2011. **25**(7): p. 2275-2296.
62. Platten, M., J. Wright, J. Cooper, and G. Dimitriadis, *Identification of a nonlinear wing structure using an extended modal model.* Journal of Aircraft, 2009. **46**(5): p. 1614-1626.
63. Londoño, J.M., J.E. Cooper, and S.A. Neild, *Identification of systems containing nonlinear stiffnesses using backbone curves.* Mechanical Systems and Signal Processing, 2017. **84**: p. 116-135.